Acta Biomaterialia 73 (2018) 559–566

Contents lists available at ScienceDirect

Acta Biomaterialia

journal homepage: www.elsevier.com/locate/actabiomat

Full length article

In vivo quantification of hydrogen gas concentration in bone marrow surrounding magnesium fracture fixation hardware using an electrochemical hydrogen gas sensor

Daoli Zhao [a,1], Andrew Brown [b,c,d,1], Tingting Wang [a], Sayuri Yoshizawa [b,c], Charles Sfeir [b,c,d,e,*], William R. Heineman [a,*]

[a] Department of Chemistry, University of Cincinnati, 301 Clifton Court, Cincinnati, OH 45221-0172, USA
[b] Department of Periodontics and Preventative Dentistry, University of Pittsburgh, 3501 Terrace Street, Pittsburgh, PA 15261, USA
[c] The Center for Craniofacial Regeneration, University of Pittsburgh, 335 Sutherland Drive, Pittsburgh, PA 15261, USA
[d] Department of Bioengineering, University of Pittsburgh, 3700 O'Hara Street, Pittsburgh, PA 15261, USA
[e] The McGowan Institute for Regenerative Medicine, 450 Technology Drive, University of Pittsburgh, Pittsburgh, PA 15219, USA

ARTICLE INFO

Article history:
Received 2 November 2017
Received in revised form 9 April 2018
Accepted 18 April 2018
Available online 20 April 2018

Keywords:
Magnesium
MicroCT
Fixation devices
Fracture fixation
Amperometric hydrogen sensor

ABSTRACT

Magnesium (Mg) medical devices are currently being marketed for orthopedic applications and have a complex degradation process which includes the evolution of hydrogen gas (H_2). The effect of H_2 exposure on relevant cell types has not been studied; and the concentration surrounding degrading Mg devices has not been quantified to enable such mechanistic studies. A simple and effective method to measure the concentration of H_2 in varying microenvironments surrounding Mg implants is the first step to understanding the biological impact of H_2 on these cells. Here, the *in vivo* measurement of H_2 surrounding fracture fixation devices implanted *in vivo* is demonstrated. An electrochemical H_2 microsensor detected increased levels of H_2 at three anatomical sites with a response time of about 30 s. The sensor showed the H_2 concentration in the bone marrow at 1 week post-implantation (1460 ± 320 μM) to be much higher than measured in the subcutaneous tissue (550 ± 210 μM) and at the skin surface (120 ± 50 μM). Additionally, the H_2 concentrations measured in the bone marrow exceeded the concentration in a H_2 saturated water solution (~800 μM). These results suggest that H_2 emanating from Mg implants in bone during degradation pass through the bone marrow and become at least partially trapped because of slow permeation through the bone. This study is the first to identify H_2 concentrations in the bone marrow environment and will enable *in vitro* experiments to be executed at clinically relevant H_2 concentrations to explore possible biological effects of H_2 exposure.

Statement of Significance

An electrochemical H_2 sensor was used to monitor the degradation of a Mg fracture fixation system in a lapine ulna fracture model. Interestingly, the H_2 concentration in the bone marrow is 82% higher than H_2 saturated water solution. This suggests H_2 generated in situ is trapped in the bone marrow and bone is less permeable than the surrounding tissues. The detectable H_2 at the rabbit skin also demonstrates a H_2 sensor's ability to monitor the degradation process under thin layers of tissue. H_2 sensing shows promise as a tool for monitoring the degradation of Mg alloy *in vivo* and creating *in vitro* test beds to more mechanistically evaluate the effects of varying H_2 concentrations on cell types relevant to osteogenesis.

1. Introduction

Biodegradable implants for fracture fixation offer many advantages over the permanent stainless steel and titanium devices widely used today [1–10]. Importantly, implants based on biodegradable materials provide mechanical support during bone

* Corresponding authors at: Department of Periodontics and Preventative Dentistry, University of Pittsburgh, 3501 Terrace Street, Pittsburgh, PA 15261, USA (C. Sfeir). Department of Chemistry, University of Cincinnati, 301 Clifton Court, Cincinnati, OH 45221-0172, USA (W.R. Heineman)

E-mail addresses: csfeir@pitt.edu (C. Sfeir), William.Heineman@uc.edu (W.R. Heineman).

[1] These authors contributed equally to this work.

https://doi.org/10.1016/j.actbio.2018.04.032
1742-7061/

healing and are designed to degrade at a time following sufficient increases in regenerated bone strength, eliminating the need for surgically removing the devices later if complications arise. Magnesium (Mg) based alloys are promising candidates for biodegradable implants used for fracture fixation and other orthopedic and craniomaxillofacial applications due to their biocompatibility, suitable rate of degradation, and similar mechanical properties to cortical bones [7,8,11–18]. In addition to providing mechanical strength while bone is regenerating, Mg alloys have been found to enhance bone regeneration compared to titanium and polymer control devices [8,19,20].

It is known that Mg and its alloys degrade in aqueous environments, generating magnesium (Mg^{2+}) and metallic alloying element ions, hydroxide (OH^-) ions, as well as hydrogen (H_2) gas.

$$Mg + 2H_2O \rightarrow Mg^{2+} + 2OH^- + H_2$$

Mg and its alloys have been used in pre-clinical animal studies evaluating fracture fixation and ACL graft fixation with different devices such as plates, screws, and pins [19–26]. These studies used a combination of radiographic (micro-computed tomography and X-ray imaging) and histological methods to assess the degradation of the Mg devices and their impact on surrounding tissues and cells. Some of these studies describe accumulation of gas pockets surrounding the Mg implants. However, the generation of H_2 gas was not measured nor was its distribution throughout the various tissues surrounding the implants assessed. Additionally, Bartsch et al. measured pH changes surrounding Mg devices implanted *in vivo* by fluorescence imaging, but this method required the injection of fluorescent dye seminaphthorhodafluor [27]. Several research groups have extrapolated Mg device degradation rates to Mg^{2+} concentrations observed by cells *in vivo* to begin exploring the molecular mechanisms underlying the enhanced bone regeneration observed around Mg devices which highlights the importance of understanding and identifying the presence of the alloys' various degradation products within the healing environment [25,28,29]. However, no studies exist that assess the impact of H_2 on the behavior of cells relevant to fracture healing (osteoblasts, osteoclasts, bone marrow stromal cells, etc.).

Since one molecule of H_2 generated is liberated for one metallic Mg atom that degrades, measuring the evolved H_2 allows a direct measurement reflecting the degradation of Mg [30]. In addition to enabling definition of Mg alloys' degradation products within the biological environment for mechanistic studies, direct and non-invasive measurement of Mg device degradation while implanted in the body would enable monitoring to ensure that device degradation was proceeding appropriately given the related bone regeneration. Monitoring the degradation of a Mg device is frequently done *in vivo* using radiographic measures such as microcomputed tomography (MicroCT) and X-ray imaging, however, these techniques require major equipment and exposure to X-ray absorption and their sensitivities are limited. MicroCT can be used for *in vivo* imaging, but typically only in small animal models.

Recently, we have demonstrated that the measurement of H_2 generated by degradation of Mg and its alloys implanted subcutaneously using an electrochemical H_2 sensor *in vivo* is a simple and effective non-invasive method for monitoring H_2 concentrations transdermally in small animal models [31–35]. The H_2 concentration measured at the skin surface above the implanted alloy was found to be proportional to the weight loss of explanted implants. The faster the degradation rate of a Mg alloy, the higher the H_2 concentration that was detected. This method employed a highly sensitive H_2 electrochemical sensor and relied on the high permeability of H_2 through skin. While effective at translating observed H_2 concentration into degradation rate, these studies did not evaluate functional devices implanted in bony environments where complex tissues' varying H_2 diffusion rates likely impact the accumulation of H_2.

This study aims to monitor the degradation of a Mg fracture fixation system in a lapine ulna fracture model using electrochemical sensors for H_2 gas. A more comprehensive and quantitative assessment of H_2 distribution within varying tissue environments surrounding implants could lead to improved understanding of the mechanisms underlying the enhanced bone regeneration observed surrounding a Mg device, as well as the factors contributing to the accumulation versus dispersion of H_2 degradation byproducts. Completion of this study would serve as the first step in establishing a test bed for evaluating the impact of H_2 exposure, at clinically relevant H_2 concentrations, on cell populations exposed to degrading Mg devices.

2. Experimental

2.1. Device design and fabrication

The device fabrication process follows our earlier procedure [19]. Mg rod stock (99.9% Mg, Goodfellow, PA) was subjected to CNC machining to produce fixation plates (4.5 × 20 mm) with four holes for fixation screw placement and screws that were 7 mm long with a shaft outer diameter of 1.75 mm. Fixation plates as-machined were then polished with 400, 600, 800 and 1200 grit diamond films. Both fixation plates as-polished, and screws as-machined were then acid etched in a solution of glycerol, acetic acid and nitric acid for 10–15 s to homogenize surface characteristics. Prior to implantation the fixation plates and screws were subjected to gamma sterilization with a dose of 20 kGy at a dose rate of 23.5 Gy/min (Mark I 68, JL Shepherd and Associates, San Fernando, CA).

2.2. Surgical implantation

A rabbit ulna fracture model was used to assess Mg device degradation in a functional orthopedic application as it is well-established in the literature [36] and has been previously used by our group [19,20]. All the animal experiments and procedures were approved by the University of Pittsburgh Institutional Animal Care and Use Committee and carried out in accordance with the NIH Guide for Care and Use of Laboratory Animals. A total of 9 New Zealand White rabbits (12 weeks old, Charles River Laboratories, Wilmington, MA) were used in the study. Right or left ulnae from forearms of eight of the nine animals were subjected to surgical implantation of the fixation plate and screw following osteotomy creation and one rabbit was used as a sham surgical control with no osteotomy created or fixation plates and screws implanted (Fig. 1).

Prior to surgery, rabbits were sedated using ketamine and xylazine, intubated and anesthetized using isoflurane, and forearms were shaved and disinfected. The skin and muscle overlying the ulnae were dissected with a scalpel and the overlying muscle was elevated and retracted to enable surgical manipulation of the ulnae. In each experimental rabbit, an osteotomy was performed at the midpoint of the ulna using a rotating burr, resulting in a defect approximately 1 mm in proximal-distal length and through the full width and height of the ulna. A plate and screw set was then implanted by drilling 4 pilot holes (2 on each side of the osteotomy site) using a hand-held drill, placing the plate across the osteotomy site, and securing in place with 4 screws such that all screws engaged cortical bone on both sides of the ulnae as shown in Fig. 2a and b. A 2 mm burr hole was then created through the anterior cortical wall, using the handheld drill, both proximal

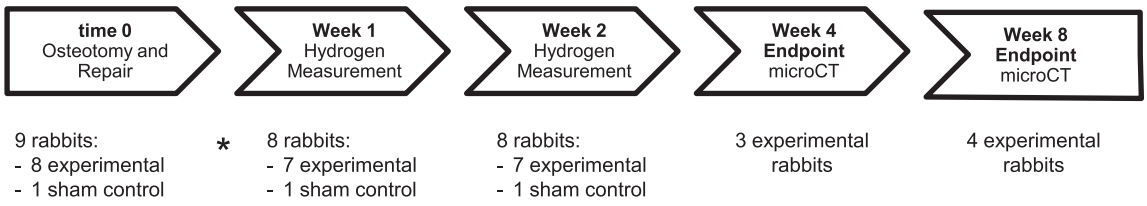

Fig. 1. Experimental timeline and sample size at each assessment. The study began with 9 total rabbits, 8 assigned to the experimental arm receiving an osteotomy and repair and 1 sham control who did not receive an osteotomy or repair. *On the third postoperative day one rabbit expired and was removed from H_2 monitoring procedures and the 4 week endpoint.

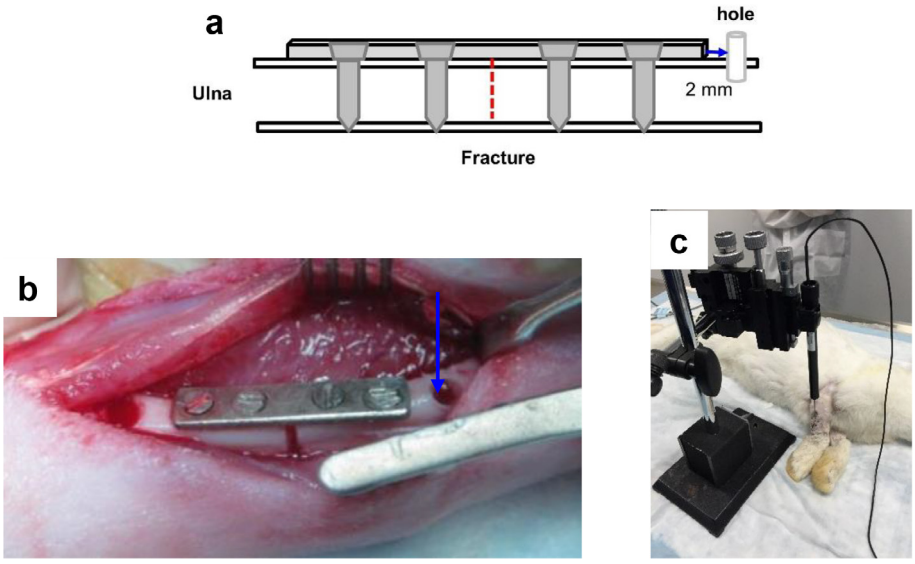

Fig. 2. (a) Schematic drawing showing placement of Mg fixation plate attached to the fractured ulna bone with four Mg screws that penetrate through the bone marrow interior. The osteotomy site (fracture) in the ulna is marked by the vertical dashed line. Sensor measurements were made by inserting the probe tip through the tissue and into the predrilled hole in the bone shown on the right (The scheme is not to scale). (b) Photograph of Mg device for fracture fixation during the implantation stage. The measuring hole for H_2 sensing is to the right of the fixation plate (marked with blue arrow). (c) H_2 microsensor assembled on a micromanipulator for measuring H_2 from Mg alloy implanted in a rabbit ulna. (For interpretation of the references to colour in this figure legend, the reader is referred to the web version of this article.)

and distal to the Mg plate to allow monitoring of H_2 evolution with the sensor. The overlying soft tissue was then closed in layers using resorbable Vicryl sutures and the location of the H_2 monitoring port was marked on the skin with a tattoo. A sham surgery was performed on one rabbit such that the osteotomy and subsequent plate and screw fixation were not performed, but a burr hole for H_2 monitoring was created.

All rabbits received post-operative Ketophen for analgesia twice a day for 3 days and Baytril for antibiotic coverage twice a day for 3 days. Rabbits also received e-collars post-operatively to prevent chewing of sutures until incision sites had healed (approximately 10 days post-op). Rabbits were monitored for general behavior, movement, and food and water intake, with standard diet and standard enrichment beginning in the immediate post-operative period. Rabbits were monitored daily for signs of lameness, lethargy, wound dehiscence and infection. This post-operative care procedure was carried out following the surgical implantation, as well as H_2 monitoring procedures.

2.3. H_2 measurement by electrochemical H_2 sensor

H_2 measurements were made with two electrochemical H_2 sensors (Unisense, Aarhus, Denmark) that operate in the amperometric mode by applying a voltage to the working electrode and measuring the current resulting from oxidation of H_2 [31–35,37]. One sensor was outfitted with a needle sensing tip (1.6 mm tip diameter, H_2-NP) and was used for measurements where the rabbit skin was penetrated, such as inside the bone marrow and the subcutaneous tissue, and for some transdermal measurements by pressing or just gently touching the tip to the rabbit skin. The other sensor was outfitted with a flat glass capillary tip (50 μm tip diameter, H_2-50) and was used for measurements made transdermally by pressing or just gently touching the tip to the rabbit skin. The amperometric microsensors were connected to a multimeter for measurements (Unisense, Aarhus, Denmark). The H_2 sensors were calibrated and the multimeter readout converted from microsensor current to H_2 concentration using a calibration curve generated from standards prepared by dilution of H_2 saturated water following our method reported earlier [31–35,37]. H_2 concentrations greater than those in saturated water were determined based on extrapolation of the calibration curve to higher concentrations.

For *in vivo* measurements, the H_2 sensors were sanitized by submerging in 70% ethanol for 5 min between animals. Rabbits were sedated using ketamine and xylazine and anesthetized using isoflurane (delivered via mask). Rabbits were maintained on a heated table where the microsensor tip was positioned for measurement with a micromanipulator as shown in Fig. 2c. Control measurements for H_2 sensing were made by inserting the needle sensor tip inside the bone marrow (using the monitoring port created proximal to the plate and screws) and the subcutaneous tissue or just touching the flat capillary sensor tip on the skin of the surgical sham control rabbit without an osteotomy or Mg implant. All measurements were conducted on all rabbits at both 1 week and 2 weeks post-surgical implantation.

Measurements in the bone marrow were made by penetrating the skin at the tattoo mark with the H_2 needle sensor and then gently pushing it through the tissue and into the hole predrilled in the bone before the implantation of the Mg plate and screws shown in Fig. 2a and b. Measurements were then made in subcutaneous tissue by withdrawing the sensor tip out of the bone and underlying tissue so that it was in contact with the subcutaneous space. Finally, H_2 was measured non-invasively on skin above the implant by pressing the H_2 sensor tip (either needle or flat capillary) against the skin covering the hole. This last measurement procedure is similar to that described for non-invasive transdermal measurements in our earlier reports [32,33]. Two techniques were used for the transdermal measurements: pressing the sensor tip to the skin to ensure a good contact with the skin and just gently touching the sensor tip to the skin. Although each measurement required only about 30 s for a steady state signal to be achieved, more stable H_2 signals with better precision were obtained by waiting for 90 s or longer.

2.4. Microcomputed tomography characterization

Four weeks (3 rabbits) or eight weeks (4 rabbits) post-osteotomy and fixation device implantation, rabbits were euthanized and the radius/ulna complex was explanted and fixed in formalin for 3 days. The sham control rabbit was not euthanized. Micro-computed tomography characterization was performed similar to methods described in Chaya, et. al. [19,20]. Microcomputed tomography scanning was performed at 10 μm voxel size, 60 kVp beam energy, 400 ms exposure, 10 frames averaged per view and 360 degrees angular range of scan (Skyscan 1172, Bruker-Skyscan, Belgium). Raw scan files were then reconstructed with Recon and analyzed using CTAn (Skyscan). Device volume was measured by manually defining regions of interest around all screws and plates and then setting upper and lower threshold levels for binarisation that separated the devices from the surrounding soft and hard tissues. The lower threshold levels were determined by selecting the inflection point between the maximum value of the soft tissue and background histogram curve and the maximum value of the Mg device histogram curve (average 58 ± 4 a.u.). Three-dimensional reconstruction and cross-sectional views were also obtained for qualitative characterization.

2.5. Statistical analysis

All data are expressed as the mean ± SD (standard deviation) unless indicated otherwise. For statistical analysis of H_2 generated by the Mg alloy corrosion, measurements were made on 7 experimental rabbit forearms, and one sham rabbit forearm. The statistical analysis was performed using GraphPad Prism 3 software (GraphPad Prism Software, Inc.). Statistical significance of differences between the same location at different time points and the measurement by different sensors was assessed by the student *t*-test. *P* values less than 0.05 were considered statistically significant.

3. Results and discussion

The overall goal of this research was to characterize the H_2 concentrations in the environment surrounding a functional Mg implant system in a clinically relevant animal model. Specifically, this study determined that H_2 accumulates at high concentrations within the bone marrow and then decreases in the surrounding subcutaneous space and decreases further on the cutaneous surface in the setting of the bone fracture fixation model. Furthermore, the concentrations of H_2 measured in this model were significantly higher than the concentrations of H_2 within a saturated solution of water.

Surgical implantation of plates and screws was uneventful for all rabbits. However, one rabbit was found expired in its cage on post-operative day 3 due to unknown causes. This rabbit was designated for the four-week endpoint and was thus excluded from further assessments. All other rabbits had uneventful healing courses and exhibited no signs of distress or infection with the aforementioned analgesia and antibiotic plan.

The H_2 sensor responses to positioning the tip in bone marrow, in subcutaneous tissue, pressing skin and gently touching the skin on the rabbit after one week of implantation are shown in Fig. 3. Fig. 3a shows a representative sensor response signal for one measurement with the H_2 needle sensor on a single rabbit. The sensor response signal is current from the oxidation of H_2 versus time as the sensor is positioned at the four measurement sites. The signal was initially a very small (ca. 40 pA), flat background as the sensor was held in air for about 40 s; the sensor was then slowly pushed through the skin and into the tissue above the hole in the bone during which time the signal increased gradually to about 250 pA as it was pushed deeper into the tissue, indicating that the H_2 concentration was increasing as the hole in the bone was approached; the signal then exhibited an abrupt increase as it entered the hole where it was then held in position; and, finally, the signal leveled off to a steady value of ca. 1400 pA that reflects a much higher concentration of H_2 in the marrow. After about 200 s the sensor was withdrawn from the port, resulting in the sharp drop in sensor signal, and positioned in the subcutaneous space above the port where the signal leveled off to a steady value (ca.300 pA) that is similar to that obtained just before the sensor was pushed down into the port. At about 300 s the sensor was withdrawn from the rabbit subcutaneous tissue causing the signal to drop down to background. Then, the tip was pressed firmly against the skin above the burr hole for a measurement, the signal increases from background as the sensor is in position and levels off to a value about half (ca. 150 pA) that when it was in the subcutaneous tissue. Lastly, at about 400 s the sensor was just gently touched to the skin and the signal dropped off to a low value comparable to the initial background signal. This same pattern of signal response was obtained with the other rabbits.

Fig. 3b is a bar graph summarizing the combined results for measurements at 4 different locations (in bone marrow, in subcutaneous tissue, and transdermally by pressing skin and gently touching the skin, from left to right) on all seven experimental rabbits with the H_2 needle sensor. For this graph, the raw sensor current signals were converted to H_2 concentrations by means of a calibration plot.

The H_2 needle sensor was able to easily detect H_2 in bone marrow after one week implantation, when the concentration was 1460 ± 320 μM as shown in Fig. 3b, even though no visible gas cavity was observed. The unexpectedly high H_2 concentration in bone marrow is an important discovery. The level exceeds the highest levels that we have reported for transdermal measurements of a very rapidly biodegrading Mg alloy implanted in a subcutaneous mouse model [31–35] and exceeds that in a H_2 saturated water solution, 800 μM [38]. This very high H_2 concentration suggests that some of the H_2 generated in situ from the four screw segments in the marrow was trapped in the bone marrow, presumably because of slow permeation through the marrow space and the surrounding bone. A measured concentration level that exceeds H_2 saturated water indicates that the tissue is likely saturated with H_2 and some H_2 trapped in the bone marrow is also in the form of gas bubbles, which can have a much higher concentration of H_2. Since the sensor will measure H_2 both dissolved and in gas, the high level is attributed to the contribution from gas. It also suggests that the generation of H_2 in the marrow is faster than it is

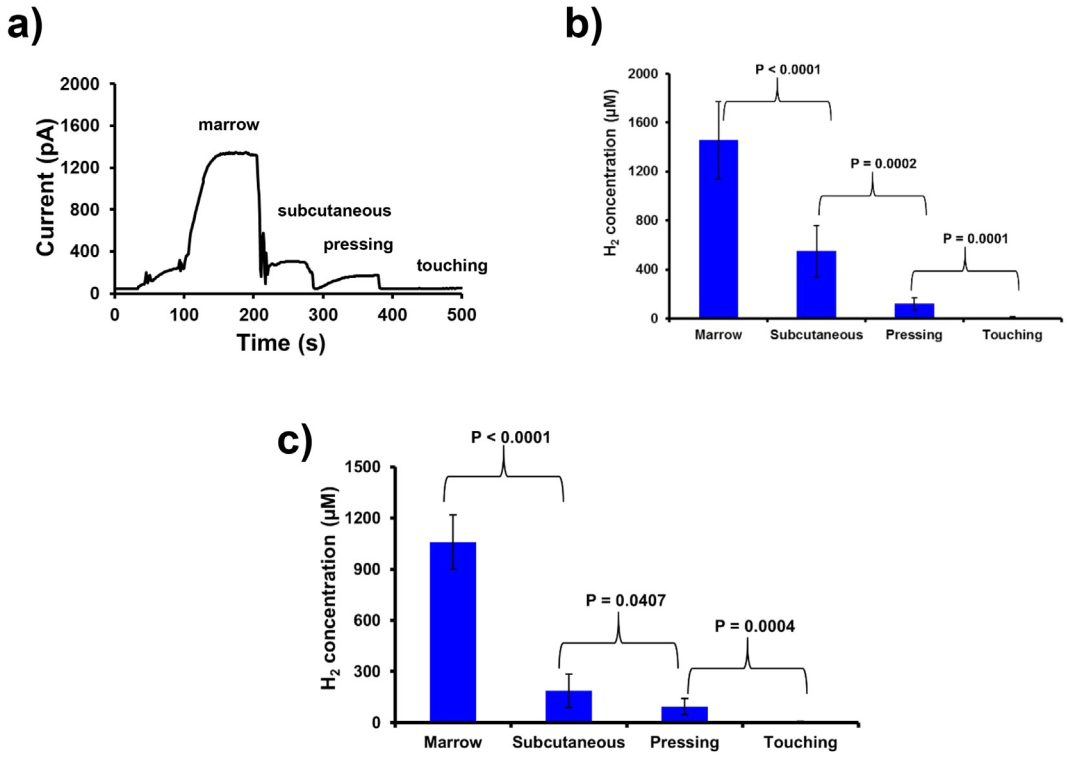

Fig. 3. H_2 measurements on anesthetized rabbits with Mg device. (a) Sensor current signal versus time for H_2 concentrations measured in bone marrow, in subcutaneous tissue, and transdermally by pressing skin and gently touching the skin (from left to right) on a single representative rabbit after 1 week implantation. (b) Average H_2 concentrations after 1 week of implantation measured for all seven rabbits at these four points as determined from a calibration curve. (c) Average H_2 concentration for all seven rabbits with Mg devices after 2 weeks implantation. Error bars are standard deviations for measurements made on seven rabbits (n = 7).

able to dissolve in the marrow and be transported from the marrow by permeation through the bone or diffusion to the measuring hole and the fracture gap for escape. These results confirm that Mg does biodegrade in the bone marrow and that H_2 transport out of the marrow is relatively slow. H_2 gas associated with Mg implants in bone has also been observed and commented on by other researchers [8,39,40]. Witte, et al. observed gas bubbles in tissue adjacent to Mg alloys implanted in bone and attributed them to extensive diffusion of H_2 [8]. Huehnerschulte et al. did not observe gas bubbles, stating that "..gas did not leave the medullary cavity, but accumulated inside of it" [8,39,40]. Wolters et al. have studied H_2 generation *in vitro* from a plate and screw system using conventional H_2 capture techniques [41]. However, there have been no reports of an *in vivo* measurement of H_2 directly in the bone marrow.

By comparison, the H_2 concentration in the subcutaneous space adjacent to the bone above the port was 550 ± 210 μM, or about 3x lower. To obtain these results the sensor tip was withdrawn from the access hole back into the subcutaneous space above the hole so the probe tip was approximately equidistant from the hole and the end of the fixation plate. The H_2 detected in this region can originate from three sources: H_2 escaping from the bone marrow through the hole, H_2 formed by degradation of the plate end that is closest to the probe tip above the hole and is diffusing to the probe tip, and H_2 from corrosion within the bone marrow that is permeating through the bone and overlying muscle. The most unlikely of these is permeation through the bone, which seems more impermeable to H_2 given the high concentration found in the marrow.

The H_2 concentration dropped to 120 ± 50 μM when the electrochemical sensor was withdrawn and then pressed against the rabbit skin, non-invasively directly above the implant. This measurement indicates that some H_2 permeates from the implant through the subcutaneous tissue and the rabbit skin to the surface and that the path length for permeation of the H_2 to the skin surface has a significant effect on the concentration of H_2 measured. For transdermal measurements at the surface with the needle probe we found that the degree of pressure exerted on the probe significantly affected the H_2 signal. The measured H_2 concentration dropped to only 12 ± 5 μM when the probe was just gently touching the rabbit skin covering the predrilled hole. Although the measurement was at the same position, the apparent concentration decreased about 10 times compared to pressing the rabbit skin. We attribute this to the slanted surface of the opening in the needle probe tip, which makes it difficult to ensure complete contact with the skin surface so that H_2 cannot escape through any gap between the probe and the skin. The pressure on the H_2 sensor affects the H_2 measurements; with more pressure, more H_2 is captured by the H_2 sensor giving a higher signal. Thus, the larger concentration measured with the sensor tip pressed against the skin is more representative of the true concentration of H_2 at the skin surface.

Our previously reported transdermal measurements were all on the subcutaneous implant mouse model where the path length for H_2 diffusion to the skin surface was only through the very thin skin on the back of the mouse [31–35]. Here we have shown that some H_2 permeates through subcutaneous tissue that includes the thin muscle covering the ulna for measurement at the surface. This H_2 level at the skin surface is much lower compared to H_2 generated by Mg alloys implanted subcutaneously in the mouse model, where H_2 only has to permeate the thin mouse skin to reach the surface [32–35]. We attribute the lower concentration to the lower permeability of the rabbit skin compared to the mouse skin, which is probably due to differences in skin thickness. The thickness of the mouse whole skin is about 0.7 mm, whereas it is about 2 mm for rabbit [42,43], or about 3x thicker. Moreover, the Mg alloy

Table 1
Volume changes of plates and screws.

Device	Plates		Screws	
	Volume (mm^3)	Decrease in Volume (%)	Volume (mm^3)	Decrease in Volume (%)
As-machined	57.5	–	9.7 ± 0.4	–
4 week Endpoint	57.1 ± 0.6	0.7	8.6 ± 0.3	11.3
8 week Endpoint	54.3 ± 4.0	5.6	7.8 ± 0.4	19.6

was implanted deeper compared to the subcutaneous implant in the mouse model. Consequently, the blood flow through the muscle overlaying the implant would be expected to carry away some of the H_2 as it diffuses through tissue, further lowering the H_2 concentration at the skin surface.

As the control, H_2 measurements were made on the rabbit bone without a Mg implant. The H_2 concentration was 6 ± 3 μM and 5 ± 2 μM in the bone marrow and subcutaneous tissue, respectively. The H_2 concentration is 2 ± 1 μM when pressing the rabbit skin, whereas no H_2 was detected when only gently touching the rabbit skin. This rabbit skin background level in the control rabbit is similar to the background level in control experiments for mouse skin of 1.0–7.3 μM [33].

Since the needle point for the needle sensor is slanted, it cannot capture all the H_2 permeating through the rabbit skin at the touching point unless it is pressed to the skin at an angle so that the slanted surface is flush with the skin. Therefore, the electrochemical H_2 glass capillary sensor (H_2-50) was also used to measure the H_2 permeability through the rabbit skin above the hole. The sensor tip of the H_2 glass capillary sensor is flat and about 50 μm in diameter, which is much smaller compared to the H_2 needle sensor (1.6 mm). Due to the small, flat tip of the glass sensor, it can tightly contact with the skin and capture more H_2 per unit area. Holding the sensor vertically to the skin and pressing just enough to slightly depress the skin gave very reproducible readings, which we also found in our earlier studies on mice [33]. Indeed, the H_2 concentrations measured with the glass sensor were much higher. The H_2 concentrations were 62 ± 10 μM when only gently touching the rabbit skin covering the predrilled holes, which is ~5 times higher than with the needle probe under the same condition as mentioned earlier (12 ± 5 μM) ($p = 0.0001$). The concentration of H_2 will be even higher if the glass sensor is pressed against the rabbit skin. However, we did not press against the skin with the glassy capillary sensor due to its fragility. The glass capillary sensor can easily detect the low concentration of H_2 by simply touching the skin. Moreover, the glass sensor probe gives a more accurate reading of the concentration of H_2 at the skin surface since a considerable amount of H_2 escapes measurement with the needle probe because of poor contact with the skin. Thus, to get a better evaluation of the degradation of Mg alloys by transdermal low H_2 concentration measurement, the H_2 glass sensor is recommended.

Fig. 3c shows results from H_2 needle sensor measurements on seven rabbits after 2 weeks implantation. The H_2 concentration had dropped to 1058 ± 158 μM in the bone marrow. The H_2 concentrations are 187 ± 96 μM and 94 ± 48 μM for the subcutaneous tissue and pressing the rabbit skin, respectively. The H_2 concentration is 5 ± 3 μM for gently touching the skin. The H_2 concentrations from all these different spots are lower compared to the first week of measurement. Compared to the first week of measurement, the H_2 concentration is significantly less in the bone marrow ($p = 0.0115$), subcutaneous ($p = 0.0013$), and gently touching the skin ($p = 0.0080$). However, there is no significant difference in H_2 concentration for gently pressing the rabbit skin ($p = 0.3406$) after 1 week and 2 weeks implantation. The lower H_2 concentration in the bone marrow, subcutaneous tissue and pressing the rabbit skin suggests a lower degradation rate of the Mg alloy in the second week. The faster degradation behavior of the screw plate system in the first week than afterward was also observed for LAE442 alloy in an *in vitro* bone model [41]. This decreased generation of H_2 is expected due to the slowing corrosion caused by formation of an increasingly thick corrosion layer of $Mg(OH)_2$ and $MgCO_3$ that has been shown to coat the implant surface [32,35]. Although the generation of H_2 decreases at 2 weeks implantation compared to the first week, the H_2 concentration in the bone marrow is still higher than an H_2 saturated water solution.

MicroCT analysis revealed plate volume at the 4 week endpoint decreased from 57.5 mm^3 as machined to 57.1 ± 0.6 mm^3 at the 4 week endpoint representing a 1% average decrease in total volume ($n = 3$) (Table 1). Screw volume decreased from 9.7 ± 0.4 mm^3 as machined ($n = 8$) to 8.6 ± 0.6 mm^3 at the 4 week endpoint representing an 11% average decrease in total volume ($n = 12$). Due to the low deviations measured across the devices, only one plate and four screws as machined were scanned prior to the implantation. At the 8 week endpoint, plate volume was 54.3 ± 4.0 mm^3 ($n = 4$) and screw volume was 7.8 ± 0.4 mm^3 ($n = 15$). Due to a technical error, one screw from the eight week timepoint could not be analyzed. The screws displayed increased volume loss compared to the plates, which is similar to observations in Chaya et al. [19]. This is likely due to the increased surface area/volume ratio of the screws compared to the plate, particularly within the threaded shaft region and could also be due to the increased fluid flow within the marrow space (where the screw resides) versus the underlying muscle space (where the plate resides). The increased volume loss observed in the screws also supports the increased H_2 concentrations measured in the marrow space versus the subcutaneous tissue.

Qualitative assessment of microCT samples correlated with the quantitative evaluation (Fig. 4). The site of the osteotomy (o) remains visible 4 weeks post-surgical creation, as does the hole created for insertion of the H_2 sensor into the marrow space (h). However, by 4 weeks post-surgical creation, the H_2 sensor hole has been infiltrated with mineralized tissue, which would prevent measurement at this time point and beyond, an important consideration for future studies. Marked pitting corrosion is noted at several locations on the plate (solid arrows) while more uniform corrosion is noted on the screws, particularly loss of the threaded portion and distal ends of the screw shaft (dashed arrows). Callous formation and bone overgrowth (c) is noted and has been observed in other studies using this surgical model [19,20,44].

Limitations of this study include the inability to extrapolate H_2 concentrations to specific degradation rates that would likely be useful long-term to enable clinically relevant information to affect decision making. The H_2 monitoring technique, as performed, is invasive and requires anesthesia to perform bone marrow and subcutaneous measurements. Future developments could focus on creating less invasive methods to perform more comprehensive characterizations of H_2 concentration in different tissue environments. The effect of varying concentrations of H_2 gas on the various affected cell populations is also not well understood. Future studies may involve *in vitro* work to understand mechanisms affected by varying H_2 concentrations, as well as the evaluation of Mg alloys with varying degradation rates in order to determine the ability

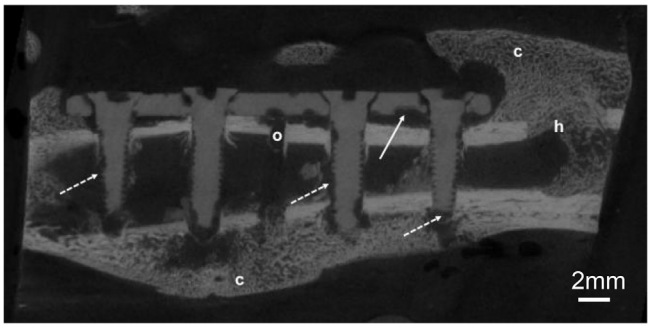

Fig. 4. Representative microCT cross-section of an ulnae explanted 4 weeks post-osteotomy and fixation with Mg plates and screws. The osteotomy site (o) remains visible however callous formation is also visible (c). The H_2 monitoring hole (h) is noted to now be infilled with bone. Device degradation is noted on both the plate (solid arrow) and screws (dashed arrows) (n = 3).

of the described H_2 monitoring technique to determine differences in degradation rate. In addition, due to the low cost, the X-ray analysis in the future experiments will be considered. More intermediate measurement time points will be performed to provide an additional clinical information on the device degradation, bone regeneration and H_2 gas cavity development.

4. Conclusion

The degradation of a Mg alloy in the bone fracture fixation model in rabbit ulnae was investigated by an electrochemical H_2 sensor. The H_2 concentration in the bone marrow was much higher than previous *in vivo* studies where H_2 was measured transdermally with Mg alloys with the subcutaneous mouse model. These results suggest that H_2 generated from degradation of the Mg screw segment inside the marrow was trapped in the bone marrow. The H_2 concentration was found to be significant, but substantially lower in the subcutaneous tissue above the plate. Although the H_2 concentrations obtained by non-invasive transdermal measurements on the skin surface above the implant are lower, the electrochemical H_2 sensor can adequately detect H_2 at these levels when pressed against the skin. These results confirm that Mg in the marrow of the bone corrodes at an easily measurable rate and that the bone is less permeable to H_2 than the surrounding tissue, which leads to a buildup of H_2 in the bone interior. H_2 sensing shows more promise as an effective means for monitoring the degradation of Mg alloys *in vivo* with larger test animals than mice and with human patients. Based on these data many biological questions arise, such as whether there is a H_2 effect on any of the components of the healing environment. Does H_2 gas accumulation affect the extracellular matrix, cells, cell signaling? Or is it an innocuous element? Further studies on the biological effect of H_2 gas are key to further establishing the biological effects of implantable Mg devices.

Acknowledgements

The authors thank the National Science Foundation (NSF ERC 0812348) for financial support. The surgical support of Dr. Samer Zaky, as well as microCT assistance provided by Dr. Kostas Verdelis and Rong Chong is appreciated.

References

[1] P.R. Cha, H.S. Han, G.F. Yang, Y.C. Kim, K.H. Hong, S.C. Lee, J.Y. Jung, J.P. Ahn, Y.Y. Kim, S.Y. Cho, J.Y. Byun, K.S. Lee, S.J. Yang, H.K. Seok, Biodegradability engineering of biodegradable Mg alloys: Tailoring the electrochemical properties and microstructure of constituent phases, Sci. Rep. 3 (2013) 2367.

[2] S. Zhang, X. Zhang, C. Zhao, J. Li, Y. Song, C. Xie, H. Tao, Y. Zhang, Y. He, Y. Jiang, Y. Bian, Research on an Mg-Zn alloy as a degradable biomaterial, Acta Biomater. 6 (2010) 626–640.

[3] Y. Chen, Z. Xu, C. Smith, J. Sankar, Recent advances on the development of magnesium alloys for biodegradable implants, Acta Biomater. 10 (2014) 4561–4573.

[4] D. Chou, D. Hong, P. Saha, J. Ferrero, B. Lee, Z. Tan, Z. Dong, P.N. Kumta, *In vitro* and *in vivo* corrosion, cytocompatibility and mechanical properties of biodegradable Mg-Y-Ca-Zr alloys as implant materials, Acta Biomater. 9 (2013) 8518–8533.

[5] S.E. Henderson, K. Verdelis, S. Maiti, S. Pal, W.L. Chung, D.T. Chou, P.N. Kumta, A.J. Almarza, Magnesium alloys as a biomaterial for degradable craniofacial screws, Acta Biomater. 10 (2014) 2323–2332.

[6] E. Poinern, S. Brundavanam, D. Fawcett, Biomedical magnesium alloys: A review of material properties, surface modifications and potential as a biodegradable orthopaedic implant, Am. J. Biomed. Eng. 2 (2012) 218–240.

[7] F. Witte, J. Fischer, J. Nellesen, H.A. Crostack, V. Kaese, A. Pisch, F. Beckmann, H. Windhagen, *In vitro* and *in vivo* corrosion measurements of magnesium alloys, Biomaterials 27 (2006) 1013–1018.

[8] F. Witte, V. Kaese, H. Haferkamp, E. Switzer, A. Meyer-Lindenberg, C.J. Wirth, H. Windhagen, *In vivo* corrosion of four magnesium alloys and the associated bone response, Biomaterials 26 (2005) 3557–3563.

[9] Y.H. Yun, Z. Dong, N. Lee, Y. Liu, D. Xue, X. Guo, J. Kuhlmann, A. Doepke, H.B. Halsall, W. Heineman, S. Sundaramurthy, M.J. Schulz, Z. Yin, V. Shanov, D. Hurd, P. Nagy, W. Li, C. Fox, Revolutionizing biodegradable metals, Mater. Today 12 (2009) 22–32.

[10] D. Hong, P. Saha, D. Chou, B. Lee, B.E. Collins, Z. Tan, Z. Dong, P.N. Kumta, *In vitro* degradation and cytotoxicity response of Mg-4% Zn-0.5% Zr (ZK40) alloy as a potential biodegradable material, Acta Biomater. 9 (2013) 8534–8547.

[11] M.P. Staiger, A.M. Pietak, J. Huadmai, G. Dias, Magnesium and its alloys as orthopedic biomaterials: a review, Biomaterials 27 (2006) 1728–1734.

[12] F. Witte, J. Fischer, J. Nellesen, C. Vogt, J. Vogt, T. Donath, F. Beckmann, *In vivo* corrosion and corrosion protection of magnesium alloy LAE442, Acta Biomater. 6 (2010) 1792–1799.

[13] F. Witte, N. Hort, C. Vogt, S. Cohen, K.U. Kainer, R. Willumeit, F. Feyerabend, Degradable biomaterials based on magnesium corrosion, Curr. Opin. Solid St. M. 12 (2008) 63–72.

[14] R. Zeng, W. Dietzel, F. Witte, N. Hort, C. Blawert, Progress and challenge for magnesium alloys as biomaterials, Adv. Eng. Mater. 10 (2008) B3–B14.

[15] F. Feyerabend, J. Fischer, J. Holtz, F. Witte, R. Willumeit, H. Drucker, C. Vogt, N. Hort, Evaluation of short-term effects of rare earth and other elements used in magnesium alloys on primary cells and cell lines, Acta Biomater. 6 (2010) 1834–1842.

[16] S.H. Byun, H.K. Lim, S.M. Kim, S.M. Lee, H.E. Kim, J.H. Lee, The bioresorption and guided bone regeneration of absorbable hydroxyapatite-coated magnesium mesh, J. Craniofac. Surg. 28 (2017) 518–523.

[17] J.W. Lee, H.S. Han, K.J. Han, J. Park, H. Jeon, M.R. Ok, H.K. Seok, J.P. Ahn, K.E. Lee, D.H. Lee, S.J. Yang, S.Y. Cho, P.R. Cha, H. Kwon, T.H. Nam, J.H. Lo Han, H.J. Rho, K. S. Lee, Y.C. Kim, D. Mantovani, Long-term clinical study and multiscale analysis of *in vivo* biodegradation mechanism of Mg alloy, Proc. Natl. Acad. Sci. U.S.A. 113 (2016) 716–721.

[18] H. Windhagen, K. Radtke, A. Weizbauer, J. Diekmann, Y. Noll, U. Kreimeyer, R. Schavan, C. Stukenborg-Colsman, H. Waizy, Biodegradable magnesium-based screw clinically equivalent to titanium screw in hallux valgus surgery: short term results of the first prospective, randomized, controlled clinical pilot study, Biomed. Eng. Online 12 (2013) 62.

[19] A. Chaya, S. Yoshizawa, K. Verdelis, N. Myers, B.J. Costello, D.T. Chou, S. Pal, S. Maiti, P.N. Kumta, C. Sfeir, *In vivo* study of magnesium plate and screw degradation and bone fracture healing, Acta Biomater. 18 (2015) 262–269.

[20] A. Chaya, S. Yoshizawa, K. Verdelis, S. Noorani, B.J. Costello, C. Sfeir, Fracture healing using degradable magnesium fixation plates and screws, J. Oral. Maxil. Surg. 73 (2015) 295–305.

[21] B. Schaller, N. Saulacic, T. Imwinkelried, S. Beck, E.W.Y. Liu, J. Gralla, K. Nakahara, W. Hofstetter, T. Iizuka, *In vivo* degradation of magnesium plate/screw osteosynthesis implant systems: Soft and hard tissue response in a calvarial model in miniature pigs, J. Cranio. Maxill. Surg. 44 (2016) 309–317.

[22] P. Cheng, P. Han, C. Zhao, S. Zhang, H. Wu, J.H. Ni, P. Hou, Y. Zhang, J. Liu, H. Xu, S. Liu, X. Zhang, Y. Zheng, Y. Chai, High-purity magnesium interference screws promote fibrocartilaginous entheses regeneration in the anterior cruciate ligament reconstruction rabbit model via accumulation of BMP-2 and VEGF, Biomaterials 81 (2016) 14–26.

[23] D. Zhao, S. Huang, F. Lu, B. Wang, L. Yang, L. Qin, K. Yang, Y. Li, W. Li, W. Wang, S. Tian, X. Zhang, W. Gao, Z. Wang, Y. Zhang, X. Xie, J. Wang, J. Li, Vascularized bone grafting fixed by biodegradable magnesium screw for treating osteonecrosis of the femoral head, Biomaterials 81 (2016) 84–92.

[24] B. Schaller, N. Saulacic, S. Beck, T. Imwinkelried, B.T. Goh, K. Nakahara, W. Hofstetter, T. Iizuka, *In vivo* degradation of a new concept of magnesium-based rivet-screws in the minipig mandibular bone, Mat. Sci. Eng. C-Mater. 69 (2016) 247–254.

[25] Y. Zhang, J.K. Xu, Y. Ruan, M. Yu, M. O'Laughlin, H. Wise, D. Chen, L. Tian, D. Shi, J. Wang, S. Chen, J. Feng, D.H.K. Chow, X. Xie, L. Zheng, L. Huang, S. Huang, K. Leung, N. Lu, L. Zhao, H.F. Li, D. Zhao, X. Guo, K. Chan, F. Witte, H. Chan, Y. Zheng, L. Qin, Implant-derived magnesium induces local neuronal production of CGRP to improve bone-fracture healing in rats, Nat. Med. 22 (2016) 1160–1169.

[26] P. Han, P. Cheng, S. Zhang, C. Zhao, J. Ni, Y. Zhang, W. Zhong, P. Hou, X. Zhang, Y. Zheng, Y. Chai, *In vitro* and *in vivo* studies on the degradation of high-purity Mg (99.99 wt.%) screw with femoral intracondylar fractured rabbit model, Biomaterials 64 (2015) 57–69.
[27] I. Bartsch, E. Willbold, B. Rosenhahn, F. Witte, Non-invasive pH determination adjacent to degradable biomaterials *in vivo*, Acta Biomater. 10 (2014) 34–39.
[28] S. Yoshizawa, A. Brown, A. Barchowsky, C. Sfeir, Magnesium ion stimulation of bone marrow stromal cells enhances osteogenic activity, simulating the effect of magnesium alloy degradation, Acta Biomater. 10 (2014) 2834–2842.
[29] S. Minardi, B. Corradetti, F. Taraballi, M. Sandri, J. Van Eps, F.J. Cabrera, B.K. Weiner, A. Tampieri, E. Tasciotti, Evaluation of the osteoinductive potential of a bio-inspired scaffold mimicking the osteogenic niche for bone augmentation, Biomaterials 62 (2015) 128–137.
[30] A. Atrens, G. Song, M. Liu, Z. Shi, F. Cao, M.S. Dargusch, Review of recent developments in the field of magnesium corrosion, Adv. Eng. Mater. 17 (2015) 400–453.
[31] D. Zhao, T. Wang, X. Guo, J. Kuhlmann, A. Doepke, Z. Dong, V.N. Shanov, W.R. Heineman, Monitoring biodegradation of magnesium implants with sensors, JOM-J. Min. Met. S. 68 (2016) 1204–1208.
[32] J. Kuhlmann, I. Bartsch, E. Willbold, S. Schuchardt, O. Holz, N. Hort, D. Hoche, W.R. Heineman, F. Witte, Fast escape of hydrogen from gas cavities around corroding magnesium implants, Acta Biomater. 9 (2013) 8714–8721.
[33] D. Zhao, T. Wang, J. Kuhlmann, Z. Dong, S. Chen, M. Joshi, P. Salunke, V.N. Shanov, D. Hong, P.N. Kumta, W.R. Heineman, *In vivo* monitoring the biodegradation of magnesium alloys with an electrochemical H_2 sensor, Acta Biomater. 36 (2016) 361–368.
[34] D. Zhao, T. Wang, B. Hoagland, D. Benson, Z. Dong, S. Chen, D. Chou, D. Hong, J. Wu, P.N. Kumta, W.R. Heineman, Visual H_2 sensor for monitoring biodegradation of magnesium implants *in vivo*, Acta Biomater. 45 (2016) 399–409.
[35] D. Zhao, T. Wang, K. Nahan, X. Guo, Z. Zhang, Z. Dong, S. Chen, D. Chou, D. Hong, P.N. Kumta, W.R. Heineman, *In vivo* characterization of magnesium alloy biodegradation using electrochemical H_2 monitoring, ICP-MS, and XPS, Acta Biomater. 50 (2017) 556–565.
[36] L.A. Mills, A.H.R.W. Simpson, *In vivo* models of bone repair, J. Bone Joint Surg. Br. 94b (2012) 865–874.
[37] D. Zhao, T. Wang, W.R. Heineman, Advances in H_2 sensors for bioanalytical applications, Trac-Trend Anal. Chem. 79 (2016) 269–275.
[38] T. Seo, R. Kurokawa, B. Sato, A convenient method for determining the concentration of hydrogen in water: use of methylene blue with colloidal platinum, Med. Gas Res. 2 (2012).
[39] F. Witte, A. Eliezer, S. Cohen, The history, challenges and the future of biodegradable metal implants, Adv. Mat. Res. 95 (2010) 3–7.
[40] T.A. Huehnerschulte, N. Angrisani, D. Rittershaus, D. Bormann, H. Windhagen, A. Meyer-Lindenberg, *In vivo* corrosion of two novel magnesium alloys ZEK100 and AX30 and their mechanical suitability as biodegradable implants, Materials 4 (2011) 1144–1167.
[41] L. Wolters, S. Besdo, N. Angrisani, P. Wriggers, B. Hering, J.M. Seitz, J. Reifenrath, Degradation behaviour of LAE442-based plate-screw-systems in an *in vitro* bone model, Mat. Sci. Eng. C-Mater. 49 (2015) 305–315.
[42] E.C. Jung, H.I. Maibach, Animal models for percutaneous absorption, J. Appl. Toxicol. 35 (2015) 1–10.
[43] G.D. Thorburn, B.H. Casey, G.S. Molyneux, Distribution of blood flow within the skin of the rabbit with particular reference to hair growth, Circ. Res. 18 (1966) 650–659.
[44] J. Reifenrath, A.K. Marten, N. Angrisani, R. Eifler, A. Weizbauer, *In vitro* and *in vivo* corrosion of the novel magnesium alloy Mg-La-Nd-Zr: influence of the measurement technique and *in vivo* implant location, Biomed. Mater. 10 (2015).